Revisiting asphaltenes instability predictions by probing destabiliztion using a fully immersed quartz crystal resonator

Mohamed Saidoun, Thierry Palermo, Nicolas Passade Poubat, Jean-Philippe Gingras, Carrier Hervé, Jean-Luc Daridon

Revisiting Asphaltenes Instability Predictions by Probing Destabiliztion using a Fully Immersed Quartz Crystal Resonator

Mohamed Saidoun[a,c], Thierry Palermo[b,*], Nicolas Passade-Boupat[a], Jean-Philippe Gingras[b], Hervé Carrier[c], Jean-Luc Daridon[c,**]

[a] *TOTAL SA, PERL Pôle Economique 2, BP 47 - RD 817 - 64170 LACQ, France*
[b] *TOTAL SA, CSTJF Avenue Larribau - 64018 PAU Cedex, France*
[c] *Laboratoire des Fluides Complexes et leurs Réservoirs-IPRA, UMR5150, CNRS/TOTAL/Univ Pau & Pays Adour, 64000 PAU, France*

Abstract

The method of Asphaltene Instability Trend (ASIST) was derived from London dispersions first principles and Flory-Huggins theory to model the microscopical appearance of unstable flocs using limited number of refractive index (n_D) measures on stock-tank oils (STO), series of liquid precipitants (n-alkanes) and routine PVT data [1].

In order to eliminate the tuning of the aging time of solutions in the method, the experimental protocol was modified by monitoring the signal of a fully immersed Quartz Crystal Resonator (QCR) to detect the instantaneous destabilization of asphaltenes in the surrounding media. Isothermal titrations were performed under atmospheric pressure while mixing. The test matrix was designed to vary the chain length of the n-alkanes titrant and the temperature. Subsequent refractive indices at detected conditions were used to calculate solubility parameters (δ) and to predict the instantaneous detection of unstable asphaltenes during the expansion of gas dissolved systems using the exact same immersed apparatus.

Predictions were then challenged against experimental observations of artificial live oil systems created by recombining dead oils with gas mixtures at pressures up to 1000*bar*. Isothermal Constant Mass Expansion (CME) experiments provided measured volumes as a function of pressure which served for modeling, along with the QCR sensor signal to probe the first agregation and deposition of unstable asphaltenes for each system at various conditions. Prediction results were compared to experimental detections for 2 different crude oils, temperatures ranging from 45^oC to 120^oC and gas dissolved concentrations ranging from 0 to 60 *%mol*.

Keywords: Asphaltenes instability; Pressure; Prediction; Crude oil; Quartz Crystal Microbalance

⋆using Asphaltene Instability Trend (ASIST)[1]

*Thierry Palermo
**Jean-Luc Daridon
Email addresses: thierry.palermo@total.com (Thierry Palermo), jean-luc.daridon@univ-pau.fr (Jean-Luc Daridon)

1. Introduction

Spooky stories of oil & gas industry have been centering asphaltenes in many fundamental research interests since decades. Indeed, anticipation of unstable asphaltenes fouling in upstream oil production and in refining systems is a key step in early project phase. Deposit build-up have been observed in many field cases forming localized flow restrictions in the production facilities. These macro-molecules are classified as soluble in aromatic solvents and insoluble in light n-alkanes, which are produced along with the complex mixtures defined as crude oils. Resulting from changes of pressure, temperature and subsequently volumetric composition of their surrounding media during transport, their destabilization is a precursor to deposition. Previous fundamental investigations involved mapping of two-dimensional solubility parameters of model oil and crude oil systems [2]. Based on results of a large number of crude oils, authors stated that asphaltenes stability was predominantly governed by Van Der Waals (VdW) interactions. A crude oil system contains very few permanent dipoles, for this reason generalizing VdW interactions to solely London dispersion interactions is a fair approximation. Consequently, predictive techniques of appearance of asphaltene instability were designed using laboratory measures of solvent parameters affecting dispersive forces such as densities [3, 4, 5, 6], molar volumes [7, 8, 9], volume ratios [10] or refractive indices [11, 12, 13, 1, 12].Vargas and Chapman [14] related solubility parameters to density and refractive indices of crude oil in order to predict solubility parameters of oil with gas dissolved. Summaries of existing modelization tools of the asphaltene precipitation were recently published by Subramanian et al. [15] and Wiehe [16].

Among, these models, the Asphaltene Instability Trend (ASIST) was developed from concepts mentioned above by New Mexico Institute of Mining and Technology in the frame of DeepStar consortium [11, 12]. The experimental approach uses microscopical detection of unstable asphaltenes with various liquid n- alkanes additions, limited number of refractive indices (n_D) measurements on stock-tank oils (STO) and routine PVT data to define a linear threshold of stability. The trend is extrapolated to predict the appearance of the least stable asphaltene due to light alkanes expansion during live crude oil transport in wells and pipelines. Comparisons of ASIST predictions for pressure depletion experiments performed in crude oils with dissolved gas systems have shown a very good agreement between the measurements and the model expectations [17, 18, 19]. Authors claim the existence of an optimal aging time of mixtures (ranging from 1 to 24h) after addition of liquid precipitants. Indeed the aging time was used as a tuning parameter for extrapolation to low molar volumes of precipitants in order to fit predictions to observations of flocs upon depressurization. This practice suggests that despite the linear thresholds of ASIST, the aggregation kinetics would vary on a single linear asphaltene intability trend.

However, we should note that experimental detections of particles during depressurization were carried out by near-infrared (NIR) light transmittance or by high pressure filtration which are different compared to the microscopy (used at atmospheric pressure) and can generate uncertainties subsequently causing the need to tune the aging time of ambient pressure measures. The microscopy observations of unstable asphaltenes are subject to human visual interpretation; but more importantly, as illustrated by Maqbool et al. [20], the appearance of clear particles of about 2 to 3μm is necessary to confirm the presence of unstable asphaltenes. In pressurized apparatus, the source of laser-light wavelength in NIR solid detection systems (SDS) is around 850nm while the pore size of high pressure filtration systems used was 500nm. All experimental probing techniques used to validate ASIST have a resolution comprised in the order of 0.5 to 2μm. However, since the high pressure apparatus were slightly more sensitive than microscopy, the tuning of the aging to longer times for microscopy detections to fit NIR or high pressure filtration data was expected. Therefore, we suspect that the tuning of the aging time is an artificial way to correct the difference in sensitivity of the techniques used.

On the other hand, some other authors have extensively studied the kinetics of asphaltenes destabilization and showed how long the aggregation process can take to reach micrometer sized flocs and even longer times to reach equilibrium[20, 21, 22]. They showed that the time to detect micrometer sized particles scales inversely exponentially to the concentration of precipitant added to the oil in time scales ranging from minutes to thousands of hours. In the same range of investigations; Haji-Akbari et al. [23, 24] eventually found a proportionality between the difference of solubility parameters (δ_{asph} the solubility parameter of asphaltenes, $\delta_{solution}$ the solubility parameter of the mixture solution) and a natural logarithm function of the total concentration of unstable asphaltenes called $C_1(0)$, the microscopy detection time of particles $t_{detection}$ and the viscosity μ of the media.

$$\ln(t_{detection}\sqrt{C_1(0)}/\mu) \propto \frac{1}{\delta_{asph} - \delta_{solution}} \tag{1}$$

This so-called unified model described by equation 1 reminds us that despite the very long time that asphaltenes can take to reach a micrometer detectable size, the concentration of unstable asphaltenes can be significantly high in a relatively viscous media. The relevance of small unstable aggregates to the deposition was revealed by Hoepfner and Fogler [25] [26] and Vilas Bôas Fávero et al. [27]. Indeed, significant accumulations of deposit were experimentally observed while flowing mixtures of n-heptane and crude oil for which unstable flocs had not reach a microscope detectable size (~0.5-2μm). The size of depositing particles was back-calculated from their mass diffusivities to diameters between 10 and 100nm, 5 to 100 times smaller than the detected flocs in high pressure monitoring techniques mentioned earlier. These foundings suggest that the size of unstable asphaltenes matters to potential deposition mechanisms, smaller aggregates will cause a faster deposition rate under diffusion-limited regime. One should note that the concentration of unstable particles is another significant parameter to such a deposition mechanism.

Therefore a better resolution of the detection of unstable asphaltenes was necessary and methods referred as direct detections cited above were judged not sensitive enough according to Tavakkoli et al. [28]. Consequently, an indirect method of detection was developed by these authors for ambient pressure destabilization experiments. The methodology was tested and validated using a model oil, which conveniently has a low viscosity and enables centrifuging out relatively small particles thanks to the good separation efficiency. However, higher viscosities or high pressure recombined oil fluids still would require large flocs of asphaltenes to form for their reliable detection using the latter technique. At elevated pressures, the wide-spread SDS using NIR light transmittance, the high pressure filtration mentionned earlier or even high pressure microscopy are commonly used [29, 30] but their sensitivity is much larger than the diameters of diffusing particles calculated by Vilas Bôas Fávero et al. [27].
The purpose of this study is to validate ASIST without tuning the aging time and to confirm the contribution of small particles (10-100nm) to deposition upon depressurization. Consequently we revisited the instrumentation used to detect asphaltene destabilization in ASIST and strictly applied the same data processing method. The following advantages were combined:

- instantaneously sensitive to orders of 10nm sized unstable aggregates [31, 32, 33]
- applicable to atmospheric pressure titration of crude oils with liquid n-alkanes
- applicable to depressurization of light alkanes (C1 to C4) recombined crude oils.

For that purpose, an acoustic sensor working in thickness shear mode was considered in this work. Indeed, Quartz Crystal Microbalance with Dissipation monitoring (QCM-D) is a well-known technique widely used to probe liquid adsorption of monolayer deposits or colloidal material on its surface thanks to piezo-electrical

properties of the quartz material. Its sensitivity has been advantageous to quantitatively study asphaltene destabilization [34, 35] and deposition in flow cells under atmospheric pressure[36, 37, 38, 39]. Moreover, it has been shown that QCM-D can be used in full immersion in live crude oil as a resonator (QCR) to probe fluid phase transitions and asphaltene destabilization [33, 40]. This work involves the use of the same experimental methods to define phase diagrams including asphaltene instability envelope for 2 recombined crude oils. The results obtained from high pressure measurements were then compared to predictions of the revisited version of ASIST using an immersed quartz sensor during n-alkane liquid titrations.

2. Materials & Method

2.1. Experimental revisit of ASIST

All liquid titrants (e.g., toluene and n-alkanes) were 98+% purity supplied by Sigma Aldrich. The 2 dead crude oil samples later referred to as crude oil A and crude oil B were provided by TOTAL from 2 different fields located offshore West Africa, both were free from contamination of water, solid particles, production additives or drilling fluid, their STO properties are summarized in Table 1.

Table 1: STO properties of crude A and B

Crude oil	**Density**	**Viscosity**	**Refractive Index**	**Asphaltenes content (by IP143)**
-	kg/m^3	$mPa.s$	**-**	**wt%**
crude A	898	64	1.5148	11
crude B	861.4	15.2	1.4902	4.5

All the following solubility parameters of liquid solutions were calculated by the linear proportionality to the Lorentz-Lorenz refractive index function proposed by Wang and Buckley [12]. In the following sections, equation 2 is applied to temperatures ranging from 20 to 120 °C ; we make the assumption that the predominant parameter affected by the temperature is the refractive index of the liquid solutions. According to van Laar- Lorenz definition of enthalpy, the other parameter affected by the temperature is the size of molecules. By using equation 2 at multiple temperatures we make the assumption that the distance between molecules (captured by the refractive index) is predominantly affecting the cohesive energy density and the variation in size of molecules is neglected.

$$\delta = 52.042\frac{(n_D^2 - 1)}{(n_D^2 + 2)} + 2.904 \tag{2}$$

The refractive indices (n_D) of crude oils and mixtures were measured at the wavelength of yellow Sodium D line ($589.3nm$) using a benchtop refractometer with a temperature control. The mentioned wavelength is usually chosen because it corresponds to the peak of absorption of organic matter and to a high enough frequency ($\sim 10^{15}Hz$) to assume that the subsequent total polarizability of the molecules is well represented by the electronic polarizability [41] (see equation 4 in the following section).

QCR Atmospheric pressure titration experiments.

The use of a $10nm$ sensitive instrument was decided to liberate ourselves from potential experimental and interpretation uncertainties thanks to the use of the same exact sensor during liquid titrations and during recombined oil depressurizations. The detection is instantaneous and is monitored in live while the titrations or depressurizations were carried out. As introduced, it was also meant to extend ASIST validations to a much finer detection with regards to small particles contribution to deposition. Holder mounted $3MHz$ AT-cut quartz crystal resonators are used thorough the entire results presented, each sensor was bought with

surfaces polished and electrodes made of Gold-Titanium. Resonance frequency and dissipation shifts (Δf & $\Delta\Gamma$) are both calculated by substracting the monitored signal to a reference signal; this reference was calibrated prior to each experiment in the air for consistency to account for a potential aging of sensors.
During the first step of each experiment, as illustrated by Figure 1, the quartz crystal sensor was fully immersed into a crude oil in a sealed custom glass vessel at atmospheric pressure. The mass of crude oil for each experiment was kept constant. The temperature was controlled in an oven ($\pm 0.5^{o}C$) and monitored by an inserted thermocouple probe. Titration experiments were achieved by pumping a pure titrant into the vessel at controlled flow rate while the mixture was continuously stirred at rates enabling an instantaneous mixing, ensured by visual inspection of the presence of a vortex. The volumetric rate of addition of the solvent was steadily increased in order to keep a nearly linear rate of change in the volume fraction of the titrant.

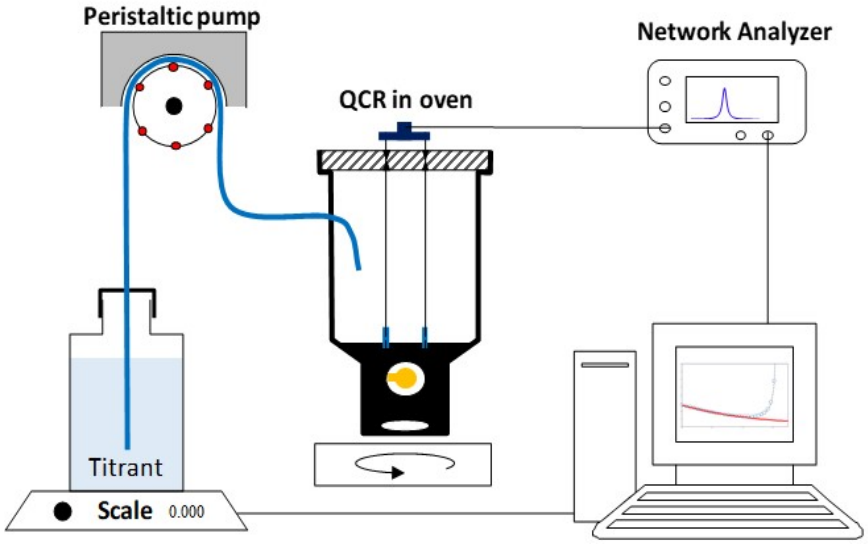

Figure 1: Atmospheric pressure experimental titration QCR set-up

While titrating the oil the electrical signal transmitted to the sensor electrodes was controlled and response was monitored through a network analyzer Agilent E5071C connected by coaxial cables to a monitor with LabVIEW internally automated program. The record of quartz frequency and dissipation signals was achieved by scans of several odd number of overtones (usually 1, 3, 5 and 7) from the first immersion and titration was started once the noise signal had reached a stable plateau ($\pm 10Hz$). As already well established by Cassiède et al. [42][43] and by Daridon et al. [35] the immersed AT-cut quartz crystals frequency of resonance is sensitive to the pressure, to the mass loaded on its surface (deposit of unstable asphaltenes) and to the contact liquid density viscosity product within a penetration depth ($\sim 100 - 300nm$) at each overtone of the nominal frequency. The dissipation of the signal is mainly affected by the ability of the surrounding media to absorb the shear waves induced by the resonance. Assuming a rigid deposit on the surface of the sensor, the dissipation is mainly affected by the density viscosity product of the mixture. The shift in resonance frequency signal was therefore chosen in order to interpret conditions of first appearance of deposited unstable asphaltenes. Treatment of the recorded raw data were performed manually and coherency of detection was further guaranteed by analyzing data of each overtone recorded. Details and validations of the detection technique used in this study are further described elsewhere [35].

2.2. *Pressurized systems experimental methods*

Sample preparation.

The high pressure experimental set up is schemed on Figure 2. It consists of a stainless steel custom jacketed and continuously stirred PVT cell with an integrated quartz crystal resonator. The equipment can undergo pressures measured through a transducer up to 1000*bar* and temperatures measured by an inserted thermocouple probe from ambient to $120^{o}C$. Pressure, volume and temperature calibration of the equipment was achieved using pure toluene prior to each experiment. Referring to previous work of Cassiède et al. [42][43] and Daridon et al. [44][45], this calibration was not only necessary to know the exact parameters of the piston cell body but also to account for the hydrostatic pressure effect on the immersed quartz sensor later referred as Δf_p .

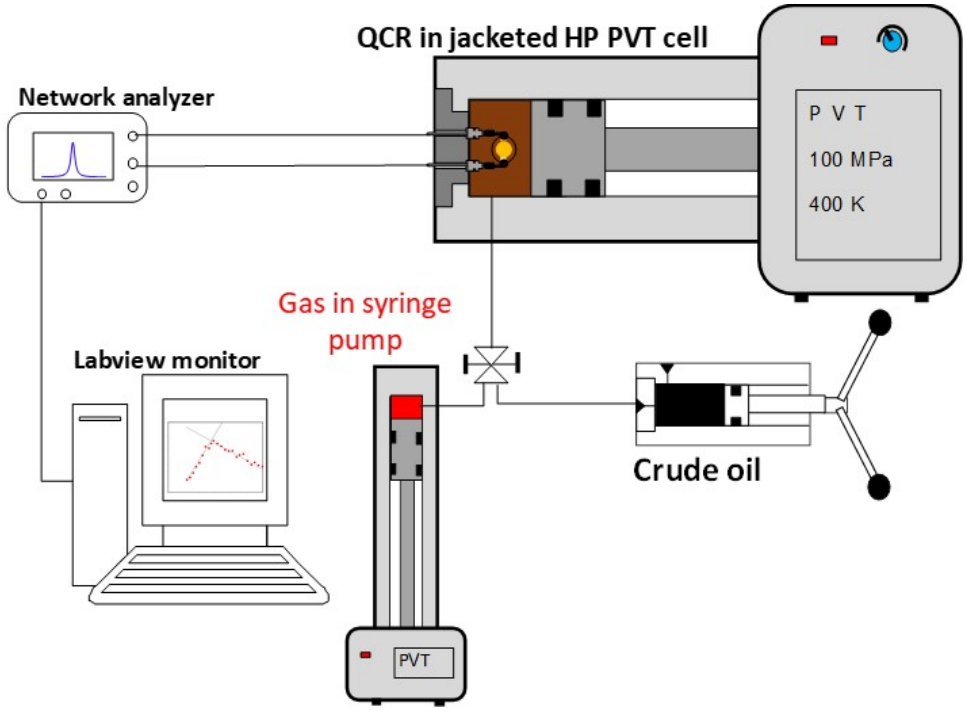

Figure 2: High pressure QCR experimental set-up

As opposed to injections of precipitant at constant pressure [8, 46], recombined oil experiments were based on the volume expansion of a constant molar composition by isothermal depressurization of a gas dissolved fluid. For such experiments, it is crucial to reduce experimental uncertainties; one of them being the control of volumes and compositions. The parameters were precisely fixed by keeping simple gas compositions with well documented thermodynamic properties of the pure methane or of the binary mixture of methane and carbon dioxide. A controlled mass of crude oil was first loaded to the PVT cell containing the sensor followed by isobar and isotherm transfer of the desired volume of the gas used as a precipitant, initially calculated using REFPROP software. Gases were supplied by Linde France SA, one bottle of pure methane and one containing a blend of methane and carbon dioxide (80:20) molar composition.

Pressure scanning.

Daridon and Carrier [33], Cardoso et al. [45] proposed a phase transition detection protocol along with a detailed treatment of recorded data to calculate the thickness of the deposited layer. These authors showed that the appearance of unstable asphaltenes and the growth of a deposit layer on the quartz crystal's surface was well correlated to the deviation from linearity of the resonance frequency shift, Δf, during pressure depletion experiments. Consequently, in our interpretation the frequency shift is used as a criterion to simplify data treatment since the detection point was the only point of interest to this study. The pressure was decreased at a rate of 3 bars per minute, a realistic depressurization rate that a fluid would experience in an oil & gas production well.

High pressure experiments.

High pressure experiments were performed at conditions summarized in Table 2 and the solubility parameter of the recombined oil solution mixtures were calculated as described in the prediction methods section. For clarity, we will only discuss results for one set of conditions investigated for the same crude oil (e. i. crude oil A recombined with 57.4%*mol* of CH_4 at 80^oC). Results at other conditions are discussed and summarized later in subsection 4.2 and in the appendix.

Table 2: Summary of the high pressure experimental range of conditions

Crude oil	**Precipitant**	**Temperature**	**Dissolved precipitant concentration**
-	**-**	^oC	**mol%**
crude A	CH_4	45 - 80	8 - 60
crude B	CH_4:CO_2(80:20)%mol	45 - 120	55 - 60

3. Theory & Calculation

3.1. Calculation of the refractive index of recombined oils

The refractive indices (n_D) at elevated pressures with gas dissolved (single liquid phase) were calculated as proposed by Buckley et al. [11], assuming a volume fraction ϕ_i averaged Lorenz-Lorentz function of 2 pseudo-components in the mixture: Stock Tank Oil (STO) and its associated gas dissolved at the respective conditions of study.

$$\left(\frac{n_D^2-1}{n_D^2+2}\right)^{P,T}_{solution} = \phi_{oil}\left(\frac{n_D^2-1}{n_D^2+2}\right)^{P,T}_{STO} + \phi_{gas}\left(\frac{n_D^2-1}{n_D^2+2}\right)^{P,T}_{gas} \tag{3}$$

The use of Clausius-Mossotti and Lorenz-Lorentz equations lets us write the equation 4 [41].

$$\left(\frac{n_D^2-1}{n_D^2+2}\right)^{P,T}_{i} = \frac{\alpha_i \rho_i^{P,T} N_0}{3 M_i \epsilon_0} \tag{4}$$

Where $\rho_i^{P,T}$ is density of component i at the pressure and temperature of test, α_i and M_i are respectively the electronic polarizability and the molecular weight of the component i, ϵ_0 is the permittivity of free space and N_0 is the Avogadro Number. By using a convenient reference condition of pressure and temperature, e. g. ambient conditions thereafter denoted by the exponent 0, Lorenz-Lorentz equation 3 combined to equation 4 leads us to the following relation which allows to calculate the refractive index function of the mixture at each pressure and temperature.

$$\left(\frac{n_D^2-1}{n_D^2+2}\right)_{solution}^{P,T} = \frac{V_{STO}^0}{V_{solution}^{P,T}}\left(\frac{n_D^2-1}{n_D^2+2}\right)_{STO}^{0} + \frac{N_{gas}}{V_{solution}^{P,T}} Rm_{gas}^0 \tag{5}$$

Where V_{STO}^0 and $V_{solution}^{P,T}$ are respective volumes of oil at reference conditions and volume of the solution mixture at the pressure and temperature of test, N_{gas} and Rm_{gas}^0 are respectively the molar quantity and the molar refractivity of the gas dissolved.

We should note that this relation assumes molecular polarizabilities of components to be independent of pressure and temperature in our range of conditions (1 to 1000 *bar* and 20 to 120^oC). Indeed, the density of the mixture is the only pressure and temperature dependent parameter in the equation 4. In our case the density is a measured value for single liquid phase conditions, i. e. at pressures greater than the saturation pressure. One can note that at under saturated pressures, the apparition of a gas phase no longer enables us to precisely measure the volume of the liquid phase and the molar quantity of gas dissolved accurately. This reinforces the choice of constant mass expansion instead of compression or constant pressure experiments to destabilize the asphaltenes.

3.2. Calculation of the molar volume of gas dissolved

Linear extrapolation of ASIST method was empirically found on the plot of solubility parameter at detection against molar volumes of the precipitants. Although mixtures of crude oil and liquid solvents are certainly not completely ideal mixtures, it is still a fair approximation to say that the molar volumes of the pure n-heptane (later referred as n-C7), n-undecane (n-C11) and n-pentadecane (n-C15) have the same values as when mixed to crude oil at atmospheric pressure. Therefore, for these liquid precipitants, their molar volumes were retrieved from the NIST database.

Unlike these components, $v_{gas}^{P,T}$ the molar volume of light compressible alkanes can be significantly different when dissolved in crude oil at elevated pressures compared to their pure properties reported in databases. Therefore, we back-calculated these values from experimental measurement. An internally TOTAL developed PVT simulator was used to calculate the density of the crude oil at pressures and temperatures of tests. We tuned binary parameters of the Peng-Robinson cubic equations of state (P-R EoS) in order to match density measurements from an Anton Paar DMA 4500 M density meter at several temperatures. Simulations were then performed to replicate results obtained during tests on drill stem tests (DST) downhole fluid samples to check the reliability of the parameters tuned. PVT simulations were then computed to generate $\rho_{STO}^{P,T}$, the density of the degassed crude oil at pressures and temperature conditions of tests.

In our case, we recombined crude oils with well-known molar compositions, again in the following calculations (equation 6) we consider two pseudo-components system composed of crude oil and the associated gas. The molar volume of the gas dissolved at specific pressure and temperature condition can then be expressed as follows.

$$v_{gas}^{P,T} = \frac{V_{gas}^{P,T}}{N_{gas}} = \frac{V_{solution}^{P,T} - \frac{m_{STO}}{\rho_{STO}^{P,T}}}{N_{gas}} \tag{6}$$

We should note that $V_{solution}^{P,T}$, N_{gas} and m_{STO} the mass of crude oil are all measured parameters in our study.

4. Results & Discussions

Conventional ASIST.

This empirical method first consists of preparing mixtures of crude oil and liquid n-alkane usually referred

as precipitants. The variable parameters are the temperature, the nature of the precipitant (chain length of n- alkane) and its concentration. Passed arbitrary aging times, the mixtures are inspected by microscopy to determine the lowest concentration of precipitant at which particles can be observed as illustrated in Figure 3. In our case, the aging time of 72h was chosen only for practical reasons on the microscopy detections. These results are later compared to the revisited ASIST by immersed quartz detection of unstable asphaltenes.

Figure 3: Illustration of microscopy detection of unstable asphaltenes - crude oil A

The solution with the lowest concentrations of precipitant showing flocs of asphaltenes were reproduced to measure refractive indices and the corresponding solubility parameter are computed using equation 2. For each temperature, the solubility parameters of threshold solutions are plotted against $v_p^{1/2}$, the square root of precipitant's molar volume (see Figure 4). Upon addition of precipitants at a respective temperature, $\delta_{solution}$ decreases; a solution having a higher solubility parameter compared to the instability linear threshold (or trend) is defined as stable and ones having a smaller solubility parameter contain unstable asphaltenes because they correspond to mixtures with higher concentrations of the precipitant.
The detection threshold can then be extrapolated to both parameters of interest; the temperature and lower molar volumes of the precipitant (e. g. gas dissolved). Linear extrapolation of the inverse of temperature was used because it was observed to be in fair agreement with experimental data in the range investigated. Results of the applied conventional ASIST method are plotted in Figure 4.

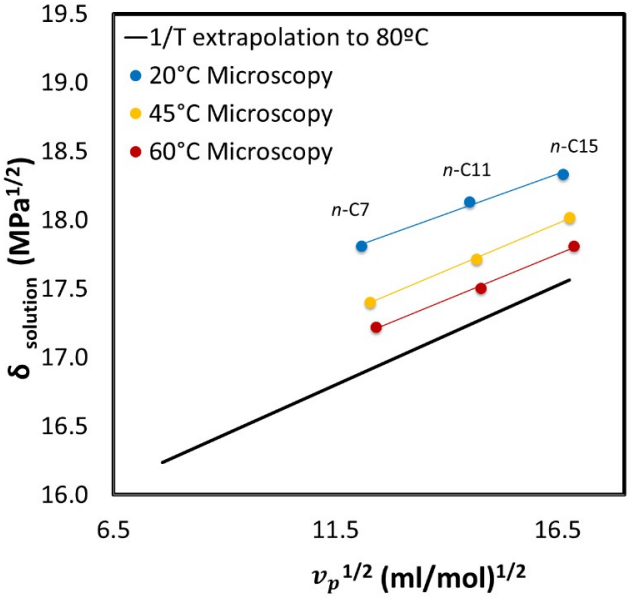

Figure 4: ASIST applied to crude oil A by microscopy detection of unstable asphaltenes(aging time of 72h)

The experimental concept of an optimal aging time (here arbitrarily chosen to be 72h) discussed by several authors brings questionable uncertainties to the method as discussed in the introduction[17, 18, 19]. Indeed, the kinetics of asphaltenes' aggregation depends on the precipitant causing the instability [23], however the definition of the instability trends of ASIST suggests that the aging time should be kept constant in the empirical inputs along the entire trend. Therefore, the extrapolation of thresholds to lower molar volume of precipitant should involve similar aging time to any precipitant. In the present study, we suspected that the necessary tuning of the aging time could be due to the difference sensitivity of instrumentations used to probe the presence of flocs in solutions at atmospheric pressure and at gas dissolved pressurized conditions.

QCR atmospheric titration results. Crude oil A was titrated by a good solvent, toluene, and a precipitant, n-C7 at the exact same conditions of stirring, injection and temperature in 2 distinct experiments. The Figure 5(a) shows the results of the frequency shift evolution for both experiments.

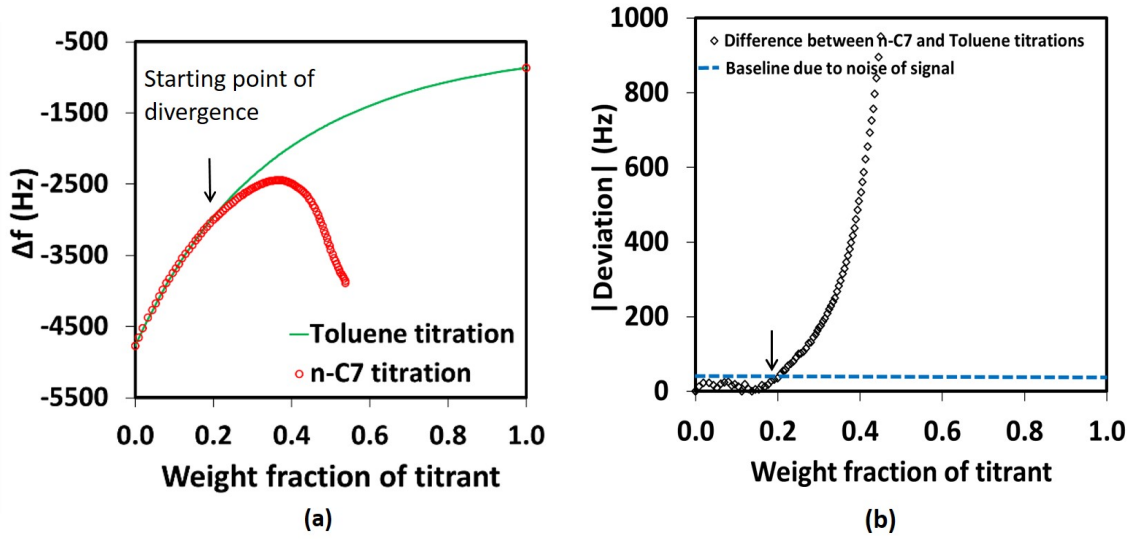

Figure 5: **(a)** Δf signal recorded for titration experiments of crude oil B at 20^oC – **(b)** difference between Δf signals of n-C7 and toluene titrations

By considering that no mass was accumulated on the surfaces during the titration of a good solvent, according to equations established by Kanazawa and Gordon [47], the change in frequency shift for a quartz oscillator is proportional to the change of the density viscosity product of the contacting liquid for homogeneous systems with no adsorption or deposition later referred as mass loading effects:

$$\Delta f_{n,\mu} = -\sqrt{n}\frac{C_m}{\sqrt{\pi f_0}}\sqrt{\rho_{liq}\mu_{liq}} \tag{7}$$

$$C_m = \frac{2f_0^2}{\sqrt{\rho_q \mu_q}} \tag{8}$$

Where C_m is the Sauerbrey constant defined by equation 8, f_0 is the fundamental resonance frequency of the quartz crystal used, ρ_q and μ_q are the density and the shear modulus of the quartz material and n is the overtone investigated [48].

Therefore, thanks to the similar density viscosity products of toluene and n-C7, toluene titration results provides insights of the dilution effect of n-C7. In other words, if n- C7 was a good solvent to all the compounds of the oil, its titration would result in the same data as the ones of toluene. As illustrated by the data of Figure 5(a) and 5(b), for precipitants the measured resonance frequency diverges from dilution effect upon increase of their fraction. At the interpreted detection of a divergence, the change in $\sqrt{\rho_{liq}\mu_{liq}}$ of the surrounding media and the surface mass load are two competing effects. Indeed the response is first due to the presence of particles in the vicinity of the sensor; it could be intepreted by a change in viscosity and density of the surrounding media. When the titration of precipitant is carried further, the change in slope with an opposite sign effect indicates accumulation of multiple layers deposit on the surface of the sensor as opposed to a monolayer adsorption. This effect becomes predominant compared to the presence of particles in the surrounding bulk and the dilution effects. The behavior is explained by a combination of Sauerbrey and Kanazawa equations resulting in equation 9; indeed an increase of the theoretical mass deposited per unit of area $\rho_{deposit}h_{deposit}$ makes the shift in frequency absolute value decrease while the reduction of $\sqrt{\rho_{liq}\mu_{liq}}$ due to dilution induces an increase of the absolute value $|\Delta f|$[47, 48].

$$\Delta f_{n,load} = -n2C_m\rho_{deposit}h_{deposit} - \sqrt{n}\frac{C_m}{\sqrt{\pi f_0}}\sqrt{\rho_{liq}\mu_{liq}} \tag{9}$$

The difference between both signals recorded; titration by toluene and titration by n-C7, was then computed in order to locate the lowest heptane concentration at which the signal significantly deviates from a dilution curve due to the presence of unstable asphaltenes to the vicinity of the sensor before deposit accumulates. The Figure 5b illustrates how the detection was geometrically determined by intersection on a narrowed region of weight fraction at the departure of the curve. After interpretation, the mixtures at which divergence was detected were replicated in order to measure their respective refractive indices. Results are summarized in Table 3 in the appendix .

The effect of the aging time of solutions was studied using the methodology described by Maqbool et al. [20]. Figure 6 shows how the detection time curve of unstable asphaltenes by microscopy compares to the instantaneous detection of the QCR signal while titrating. At the QCR detection conditions, we would have to age the solution $10^5 h$ in order to detect micrometer sized particles.

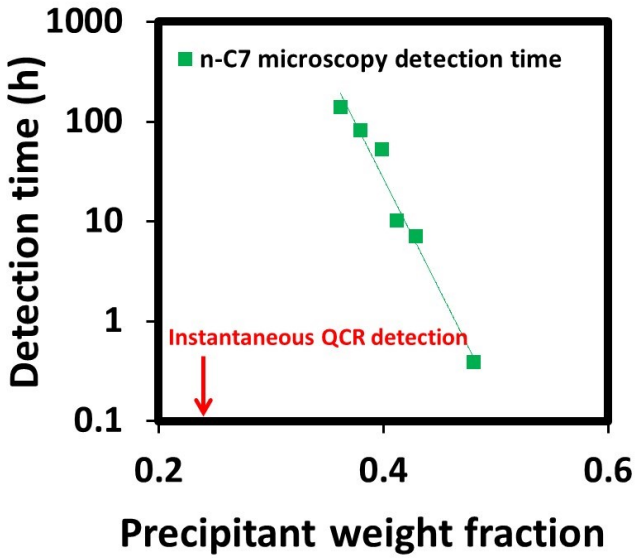

Figure 6: Comparison the detection time curve by microscopy and QCR instantaneous detection of unstable asphaltenes for crude oil A at 60°C

In a similar manner to microscopy data showed in Figure 4 and for comparison to microscopy detected trends, Figure 7 incorporates the data for crude oil A using QCR first detection of unstable asphaltenes in the vicinity of the sensor. The extrapolation to higher temperature was again achieved by an inversely linear proportionality and the range of investigated temperatures was verified to be a good approximation of a linearized inverse dependence.

As expected, larger concentrations of precipitants are required to observe flocculation through an optical microscope even aged for 72h, this is put in perspective by inferior solubility parameters required by microscopy compared to QCR detection of unstable asphaltenes at a given temperature with a given n-alkane. We can note that the results do not only show a change in the sensitivity (magnitude of $\delta_{solution}$) but also a significant change in slope of the trends against $v_p^{1/2}$. In other words, for this particular case it seems that the titration of a system contaning nanometer sized unstable asphaltenes with different precipitants requires different solubility parameter change to reach micro-aggregates. This result suggests that the nature of the precipitant has an effect on the kinetics of aggregation between nanometer and micrometer sized unstable asphaltenes. The experimental data are summarized in Table 4 of the appendix.

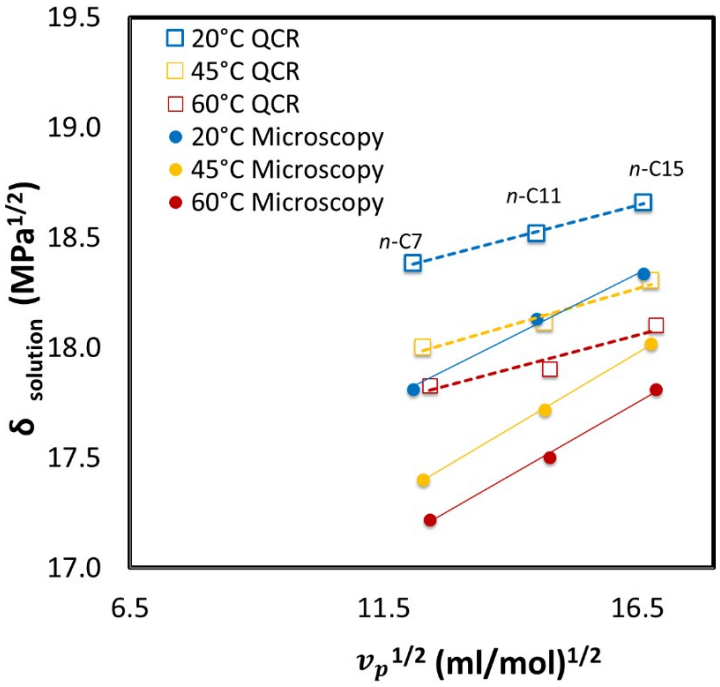

Figure 7: Comparison of ASIST using microscopy detections of unstable asphaltenes and using QCR detection of first deposit for crude oil A

4.1. Predictions of ASIST by QCR

In Figure 8, the graphical representations are showed in parallel to illustrate the data process to predict the pressure at which detection should be expected.

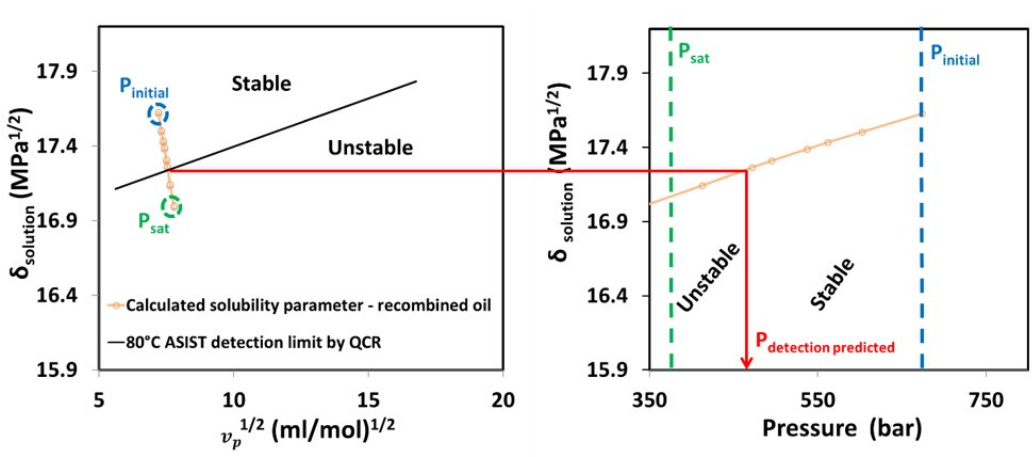

Figure 8: Prediction of the deposit detection pressure for Crude oil A recombined at $80^{o}C$ with 57.4%*mol* of CH_4

For the condition showed, the ASIST predicted pressure of appearance of unstable asphaltenes to the vicinity of the sensor is 465*bar*, the experimentally observed detection is provided in the following section along with results of different conditions.

4.2. Constant Mass Expansions experimental results

Constant mass expansion (CME) scanning results are showed in Figure 9 for two different compositions in gas content, both experiments were achieved using crude oil A at a controlled temperature of 80^oC. Figure 9(a) shows results for a system containing 29.95%*mol* of methane, frequency and dissipation shifts show as expected a sharp change in slope due to the appearance of the gas phase at the saturation pressure, confirmed by the behavior of volume of the system. Both frequency and dissipation shifts experience a monotonous linear trend before reaching the bubble pressure. Analogically to the atmospheric pressure titrations, this is due to a dilution effect of the expanding compressible components (mainly methane in this case), which induces a reduction of the $\sqrt{\rho_{liq}\mu_{liq}}$. In this case, the system passes the pressure scanning without destabilizing asphaltenes. Unlike to the system containing $29.95\%_{mol}$, the recombined crude oil with $57.4\%_{mol}$ of methane experienced a diverging frequency signal from linearity at pressures above the saturation pressure (which can still clearly be determined by the sharp changes of dissipation or volume not showed in Figure 9(b) for clarity). Such behavior of the resonance frequency was demonstrated to be a signature of the appearance of unstable asphaltene by other authors[33]. We should note that the explained combination of Sauerbrey and Kanazawa in equation 9 for atmospheric pressure titrations also applies to pressure depletion [33, 42, 43].

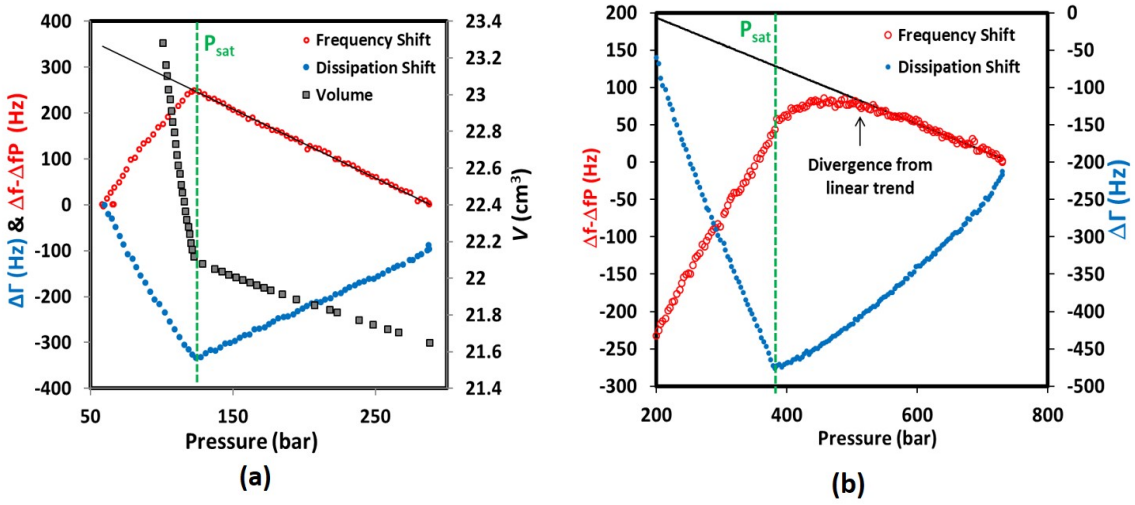

Figure 9: Depressurization experimental data recorded for crude oil A at 80 ^oC with CH_4 composition of **(a)** 29.95%*mol* and **(b)** 57.4%*mol*

The difference between the actual recorded data and the averaged linear behavior of high enough pressure data is then graphically analyzed in Figure 10 to observe the deviation and determine the experimental pressure of detection.

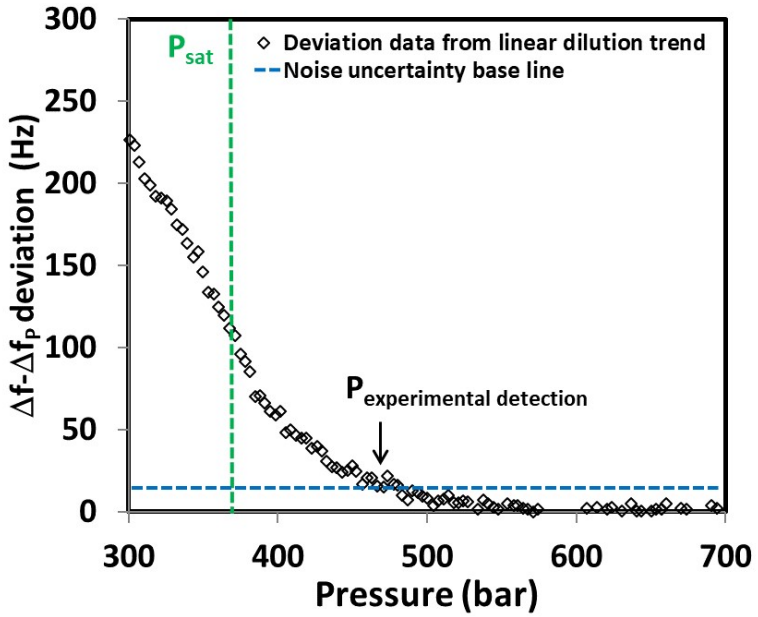

Figure 10: Deviation from linear signal due to asphaltenes instability during expansion of CH_4 (57.4%*mol*) for crude oil A at 80^oC

4.3. Comparison of predictions to experimental observations

In this section, the overall experimental data collected are compared to predictions using the modified ASIST method. All the conditions are summarized by Table 3 of the Appendix.

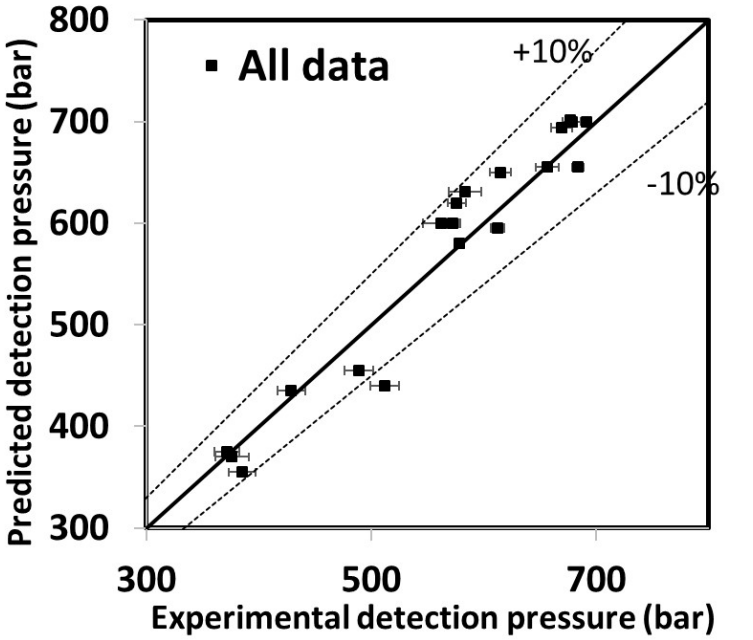

Figure 11: Revisited ASIST predictions vs experimental pressure of first deposit detected

As it can be noticed in the Figure 11, despite assumptions, potential experimental errors and theoretically unclear empirical trends, results of predicted pressures fall within ~ 10% of error compared to experimental observations. One should note additional validation results are absent from Figure 11; no detections were predicted neither observed for mixtures containing less than 55%*mol* of gas dissolved. The pressure versus temperature phase diagrams on Figure 12 show a different aspect of ASIST predictions; despite their slight offset, the curvatures follow the same trend as experimental observations, which confirms that the capture of underlying physics on the effects of temperature and pressure.

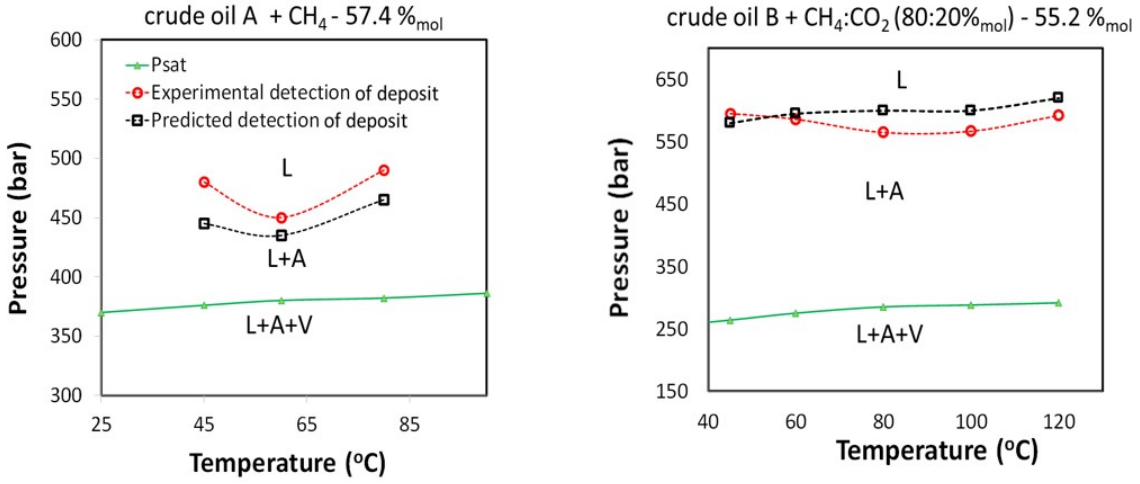

Figure 12: Pressure vs Temperature diagrams for recombined crude oils A and B. L stands for liquid, V for vapor and A for unstable asphaltenes

The conventional ASIST by microscopy and an aging time of 72h was applied to the same conditions, however, no destabilization was predicted to the depressurization experiments. This was an expected result due to the difference of resolution of the techniques.

5. Conclusions

In this study, ASIST predictive concepts were successfully implemented and revisited by using data gathered from a novel and highly sensitive method of detection of the first instantaneously unstable asphaltenes: a fully immersed Quartz Crystal Resonator (QCR). Destabilization was first caused by the volume addition of several n-alkanes in order to extrapolate to light alkanes and carbon dioxide dissolved conditions. Results of the predicted pressure at which instability would be detected using the same experimental apparatus were in excellent agreement to the actual observed detected pressures, evidencing that the tuning of the aging time is certainly an artificial matching of detections using different apparatus. This is even reinforced by the observation of a change in slope of trends depending on the size of particles, suggesting different kinetics of aggregation depending on the nature of the precipitant. In fact, using several apparatus to validate the method would add a variable. This founding do not only bring an enhanced understanding of the brutal asphaltenes destabilization during the production and transport of oil & gas, but the modified practice proposed in this publication provides prediction of different conditions at which the unstable asphaltenes are small particles that could not be detected instantaneously by microscopy but still could contribute significantly to a diffusive deposition mechanism.

Conveniently and controversially, this study shows that principles of ASIST can be applied and adapted to more or less sensitive detection methods and can give significantly different results, some of the detection techniques may be too conservative to the prediction of industrial risks while others may not be enough sensitive. It is also important to note that slight uncertainties in the measurements of compositions, refractive indices or in calculations of $\delta_{solution}^{P,T}$ and $v_{gas}^{P,T}$ at gas dissolved conditions can induce major errors in the prediction of the detection pressure. Indeed, the input parameters were randomly varied in order to observe the numerical sensitivity of the outputs. Consequently, in this study all the measurements and data processing were repeated 2 to 3 times ensuring the precision required by the method.

Although the empirical predictive tool showed excellent agreements with experimental observations, we should note that the principles of ASIST bring remarkable theoretical questions on how it relates to the extensively used Flory-Huggins regular solution theory and to other foundings. Despite the polydisperse nature of asphaltenes, the least-stable ones have hypothetically (according to the regular solution theory) a constant solubility parameter δ_{asph} for a given crude oil regardless of the precipitant used to destabilized them. However, some authors recently showed how the polydispersity can improve the modeling of unstable asphaltenes' properties [49, 50], agreeing with the extensive experimental research on the morphological structure (e. g. size, fractal dimension) of asphaltenes during precipitation[51, 52, 53, 54] which is expected to be of relevance to their transport during the deposition mechanism(s)[55, 56, 27]. In relation to the aforementionned, the predictive quantification of the destabilization and deposition of asphaltenes in gas-dissolved environment remains poorly documented. Due to the complexity of multiple variables and to the simultaneous phenomena hapenning during the flow of a live-oil, the discussed aspects in this conclusion have never been related to the asphaltenes destabilized during the expansion of light components. More comparative efforts in this direction are necessary.

6. Acknowledgements

The authors thank TOTAL SA for the financial support and the permission to publish this study.

References

[1] J. S. Buckley, J. Wang, J. L. Creek, Solubility of the least-soluble asphaltenes, Asphaltenes, Heavy Oils, and Petroleomics (2007) 401–437.

[2] I. A. Wiehe, Two-dimensional solubility parameter mapping of heavy oils, Fuel Science and Technology International 14 (1996) 289–312.

[3] N. Passade-Boupat, H. Zhou, M. Rondon-Gonzalez, Asphaltene Precipitation From Crude Oils : How To Predict It And To Anticipate Treatment?, SPE Middle East Oil and Gas Show and Conference (2010).

[4] D. Powers, H. Sadeghi, H. Yarranton, F. Van Den Berg, Regular solution based approach to modeling asphaltene precipitation from native and reacted oils: Part 1, molecular weight, density, and solubility parameter distributions of asphaltenes, Fuel 178 (2016) 218–233.

[5] H. Yarranton, D. Powers, J. Okafor, F. van den Berg, Regular solution based approach to modeling asphaltene precipitation from native and reacted oils: Part 2, molecular weight, density, and solubility parameter of saturates, aromatics, and resins, Fuel 215 (2018) 766–777.

[6] D. Barrera, D. Ortiz, H. Yarranton, Molecular weight and density distributions of asphaltenes from crude oils, Energy & fuels 27 (2013) 2474–2487.

[7] J. Wang, J. L. Creek, J. S. Buckley, Screening for potential asphaltene problems, SPE Annual Technical Conference and Exhibition (2006).

[8] K. Kraiwattanawong, H. S. Fogler, S. G. Gharfeh, P. Singh, W. H. Thomason, S. Chavadej, Thermodynamic solubility models to predict asphaltene instability in live crude oils, Energy & fuels 21 (2007) 1248–1255.

[9] H. Alboudwarej, K. Akbarzadeh, J. Beck, W. Y. Svrcek, H. W. Yarranton, Regular solution model for asphaltene precipitation from bitumens and solvents, AIChE Journal 49 (2003) 2948–2956.

[10] I. A. Wiehe, H. W. Yarranton, K. Akbarzadeh, P. M. Rahimi, A. Teclemariam, The paradox of asphaltene precipitation with normal paraffins, Energy & Fuels 19 (2005) 1261–1267.

[11] J. Buckley, G. Hirasaki, Y. Liu, S. Von Drasek, J. Wang, B. Gill, Asphaltene precipitation and solvent properties of crude oils, Petroleum Science and Technology 16 (1998) 251–285.

[12] J. Wang, J. Buckley, A two-component solubility model of the onset of asphaltene flocculation in crude oils, Energy & Fuels 15 (2001) 1004–1012.

[13] J. Wang, J. S. Buckley, Asphaltene stability in crude oil and aromatic solvents the influence of oil composition, Energy & fuels 17 (2003) 1445–1451.

[14] F. M. Vargas, W. G. Chapman, Application of the one-third rule in hydrocarbon and crude oil systems, Fluid Phase Equilibria 290 (2010) 103–108.

[15] S. Subramanian, S. Simon, J. Sjoblom, Asphaltene precipitation models: A review, Journal of Dispersion Science and Technology (2015).

[16] I. A. Wiehe, Asphaltene solubility and fluid compatibility, Energy & Fuels 26 (2012) 4004–4016.

[17] J. L. Creek, J. Wang, J. S. Buckley, et al., Verification of asphaltene-instability-trend (asist) predictions for low-molecular-weight alkanes, SPE Production & Operations 24 (2009) 360–368.

[18] D. L. Gonzalez, F. M. Vargas, E. Mahmoodaghdam, F. Lim, N. Joshi, Asphaltene stability prediction based on dead oil properties: Experimental evaluation, Energy & fuels 26 (2012) 6218–6227.

[19] S. Dolati, H. Zarei, R. Kharrat, Asphaltene Instability Trends to Predict Asphaltene Precipitation Onset Pressure: Constrained for Light and Heavy Crude Oils, Journal of Dispersion Science and Technology 36 (2015) 103–110.

[20] T. Maqbool, P. Srikiratiwong, H. S. Fogler, Effect of temperature on the precipitation kinetics of asphaltenes, Energy & Fuels 25 (2011) 694–700.

[21] T. Maqbool, S. Raha, M. P. Hoepfner, H. S. Fogler, Modeling the aggregation of asphaltene nanoaggregates in crude oil- precipitant systems, Energy & Fuels 25 (2011) 1585–1596.

[22] C. V. B. Fávero, T. Maqbool, M. Hoepfner, N. Haji-Akbari, H. S. Fogler, Revisiting the flocculation kinetics of destabilized asphaltenes, Advances in colloid and interface science 244 (2017) 267–280.

[23] N. Haji-Akbari, P. Masirisuk, M. P. Hoepfner, H. S. Fogler, A unified model for aggregation of asphaltenes, Energy & Fuels 27 (2013) 2497–2505.

[24] N. Haji-Akbari, P. Teeraphapkul, A. T. Balgoa, H. S. Fogler, Effect of n-alkane precipitants on aggregation kinetics of asphaltenes, Energy & Fuels 29 (2015) 2190–2196.

[25] M. P. Hoepfner, H. S. Fogler, Multiscale scattering investigations of asphaltene cluster breakup, nanoaggregate dissociation, and molecular ordering, Langmuir 29 (2013) 15423–15432.

[26] M. P. Hoepfner, V. Limsakoune, V. Chuenmeechao, T. Maqbool, H. S. Fogler, A fundamental study of asphaltene deposition, Energy & fuels 27 (2013) 725–735.

[27] C. Vilas Bôas Fávero, A. Hanpan, P. Phichphimok, K. Binabdullah, H. S. Fogler, Mechanistic investigation of asphaltene deposition, Energy & Fuels 30 (2016) 8915–8921.

[28] M. Tavakkoli, M. R. Grimes, X. Liu, C. K. Garcia, S. C. Correa, Q. J. Cox, F. M. Vargas, Indirect method: a novel technique for experimental determination of asphaltene precipitation, Energy & Fuels 29 (2015) 2890–2900.

[29] A. Khaleel, M. Abutaqiya, M. Tavakkoli, A. A. Melendez-Alvarez, F. M. Vargas, et al., On the prediction, prevention and remediation of asphaltene deposition, in: Abu Dhabi International Petroleum Exhibition and Conference, Society of Petroleum Engineers, 2015, pp. 1–23.

[30] M. Haghshenas, S. Balashanmugam, D. Gonzalez, M. Pietrobon, et al., Prediction of asphaltene onset pressure from dead oil stability, in: Offshore Technology Conference, Offshore Technology Conference, 2016, pp. 1–20.

[31] A. Arnau, Y. Montagut, J. V. García, Y. Jiménez, A different point of view on the sensitivity of quartz crystal microbalance sensors, Measurement Science and Technology 20 (2009) 124004.

[32] X. Huang, Q. Bai, J. Hu, D. Hou, A practical model of quartz crystal microbalance in actual applications, Sensors 17 (2017) 1785.

[33] J.-L. Daridon, H. Carrier, Measurement of phase changes in live crude oil using an acoustic wave sensor: Asphaltene instability envelope, Energy & Fuels 31 (2017) 9255–9267.

[34] L. Goual, G. Horváth-Szabó, J. H. Masliyah, Z. Xu, Adsorption of bituminous components at oil/water interfaces investigated by quartz crystal microbalance: Implications to the stability of water-in-oil emulsions, Langmuir 21 (2005) 8278–8289.

[35] J. L. Daridon, M. Cassiede, D. Nasri, J. Pauly, H. Carrier, Probing asphaltene flocculation by a quartz crystal resonator, Energy & Fuels 27 (2013) 4639–4647.

[36] S. Subramanian, S. Simon, B. Gao, J. Sjöblom, Asphaltene fractionation based on adsorption onto calcium carbonate: Part 1: Characterization of sub-fractions and QCM-measurements, Colloids and Surfaces A: Physicochemical and Engineering Aspects 495 (2016) 136–148.

[37] M. Tavakkoli, S. R. Panuganti, F. M. Vargas, V. Taghikhani, M. R. Pishvaie, W. G. Chapman, Asphaltene deposition in different depositing environments: part 1. model oil, Energy & fuels 28 (2013) 1617–1628.

[38] M. Tavakkoli, S. R. Panuganti, V. Taghikhani, M. R. Pishvaie, W. G. Chapman, Asphaltene deposition in different depositing environments: Part 2. real oil, Energy & Fuels 28 (2014) 3594–3603.

[39] S. Campen, B. Smith, J. S. Wong, Deposition of asphaltene from destabilized dispersions in heptane-toluene, Energy & Fuels (2018).

[40] J. L. Daridon, E. Orlandi, H. Carrier, Measurement of bubble point pressure in crude oils using an acoustic wave sensor, Fluid Phase Equilibria 427 (2016) 152–160.

[41] J. N. Israelachvili, Intermolecular and Surface Forces, third edition ed., Elsevier Academic Press, 2011.

[42] M. Cassiède, J.-L. Daridon, J. Paillol, J. Pauly, Impedance analysis for characterizing the influence of hydrostatic pressure on piezoelectric quartz crystal sensors, Journal of Applied Physics 108 (2010) 034505.

[43] M. Cassiède, J.-L. Daridon, J. Paillol, J. Pauly, Characterization of the behaviour of a quartz crystal resonator fully immersed in a newtonian liquid by impedance analysis, Sensors and Actuators A: Physical 167 (2011) 317–326.

[44] J.-L. Daridon, M. Cassiède, J. Paillol, J. Pauly, Viscosity measurements of liquids under pressure by using the quartz crystal resonators, Review of Scientific Instruments 82 (2011) 095114.

[45] F. Cardoso, H. Carrier, J.-L. Daridon, J. Pauly, P. Rosa, Co2 and temperature effects on the asphaltene phase envelope as determined by a quartz crystal resonator, Energy & Fuels 28 (2014) 6780–6787.

[46] A. Hirschberg, L. deJong, A. Schipper, J. Meijer, Influence of temperature and pressure on asphaltene flocculation, Society of Petroleum Engineers Journal 24 (1984).

[47] K. K. Kanazawa, J. G. Gordon, Frequency of a quartz microbalance in contact with liquid, Analytical Chemistry 57 (1985) 1770–1771.

[48] G. Sauerbrey, Verwendung von Schwingquarzen zur Wagungdiinner Schichten und zur Mikrowagung, Zeitschrift fur Physik 155 (1959) 206–222.

[49] G. Javanbakht, M. Sedghi, W. R. Welch, L. Goual, M. P. Hoepfner, Molecular polydispersity improves prediction of asphaltene aggregation, Journal of Molecular Liquids (2018).

[50] M. Tavakkoli, S. R. Panuganti, V. Taghikhani, M. R. Pishvaie, W. G. Chapman, Understanding the polydisperse behavior of asphaltenes during precipitation, Fuel 117 (2014) 206–217.

[51] L. Barré, S. Simon, T. Palermo, Solution properties of asphaltenes, Langmuir 24 (2008) 3709–3717.

[52] J. Eyssautier, P. Levitz, D. Espinat, J. Jestin, J. Gummel, I. Grillo, L. Barré, Insight into asphaltene nanoaggregate structure inferred by small angle neutron and x-ray scattering, The Journal of Physical Chemistry B 115 (2011) 6827–6837.

[53] J. Eyssautier, D. Frot, L. Barré, Structure and dynamic properties of colloidal asphaltene aggregates, Langmuir 28 (2012).

[54] Y. Yang, W. Chaisoontornyotin, M. P. Hoepfner, The Structure of Asphaltenes During Precipitation Investigated by Ultra-Small-Angle X-ray Scattering, Langmuir (2018) acs.langmuir.8b01873.

[55] W. Chaisoontornyotin, N. Haji-Akbari, H. S. Fogler, M. P. Hoepfner, Combined Asphaltene Aggregation and Deposition Investigation, Energy and Fuels 30 (2016) 1979–1986.

[56] Q. Guan, Y. Yap, A. Goharzadeh, J. Chai, F. Vargas, W. Chapman, M. Zhang, Integrated one-dimensional modeling of asphaltene deposition in wellbores/pipelines, in: Modeling, Simulation, and Applied Optimization (ICMSAO), 2017 7th International Conference on, IEEE, 2017, pp. 1–6.

Appendix

Table 3: : Experimental QCR detection results for atmospheric titration of liquid precipitants

Crude oil -	**Precipitant** -	**Temperature** ^oC	**Precipitant concentration weight%**	**Refractive Index** -
crude A	n-C7	20	24	1.4846
		45	23	1.4708
		60	24	1.4644
	n-C11	20	26	1.4896
		45	26	1.4748
		60	26	1.4672
	n-C15	20	22	1.4948
		45	23	1.4818
		60	23	1.4744
crude B	n-C7	20	20	1.4710
		45	20	1.4580
		60	20	1.4527
	n-C11	20	24	1.4765
		45	24	1.4615
		60	24	1.4558
	n-C15	20	20	1.4793
		45	21	1.4677
		60	21	1.4633

Table 4: Experimental QCR gas dissolved detection results compared to predictions using revisited ASIST

Crude oil	Precipitant	Temperature	Dissolved precipitant concentration	Experimental detection pressure	ASIST predicted pressure
-	-	oC	mol %	bar	bar
crude A	C1	45	8.27		
			20.01		
			29.95	No detection	No prediction
			39.84		
			50.02		
			55.19	376	370
			57.41	512	440
		60	8.27		
			20.01		
			29.95	No detection	No prediction
			39.84		
			50.02		
			55.19	371.5	375
			57.41	429	435
		80	8.27		
			20.01		
			29.95	No detection	No prediction
			39.84		
			50.02		
			55.19	385	355
			57.41	489	455
			59.90	583.5	631
crude B	C1:CO2(80:20) % mol	45	55.22	578.5	580
			58.12	684	655
		60	55.22	612.5	595
			58.12	677	701
			60.01	691	700
		80	55.22	572.5	600
			58.12	656.5	655
			60.01	669.5	694
		100	55.22	562.5	600
			58.12	615	650
			60.01	679	700
		120	55.22	576	620